SCA-9902

Application of Low Invasion Coring and Outcrop Studies to Reservoir Development Planning for the Villano Field

J. J. Rathmell, ARCO Technology and Operations Services, Laura K. Atkins, ARCO Dubai, Inc., and James G. Kralik, ARCO Technology and Operations Services

This paper was prepared for presentation at the Sixth Latin American and Caribbean Petroleum Engineering Conference held 21 to 23 April, 1999, in Caracas, Venezuela.

Abstract

Drilling and coring of a discovery well in the Hollin sand, Villano Field in 1992 was followed by low invasion coring in a confirmation well. A large discrepancy existed between water saturation derived from the capillary pressure and well logs in the discovery well. Low invasion coring and outcrop studies were implemented to provide the data to calculate oil-in-place and hydrocarbon reserves.

The field is located in environmentally sensitive rain forest. Low invasion coring with water based mud was the only feasible method for obtaining connate water saturation from core. The bromide tracer of mud filtrate indicated low invasion (<10 % pv filtrate) was found in 86% of the horizontal core plugs. Core plugging and preservation were conducted in a facility established at the drilling base camp, 30 minutes by helicopter from the rig.

These plugs were then shipped to the USA for analysis. Core water saturation was in good agreement with capillary pressure tests. The low invasion core data indicated salinity varied from 2600 ppm chloride at water-oil contact to 36,000 ppm chloride at the top of the Hollin reservoir. This salinity gradient and native-state, Archie saturation exponent yielded log-derived water saturation equal to the low invasion core values.

Reservoir description would be critical to a development plan for the field, which would produce by aquifer influx. The size and distribution of sand bodies and shales was addressed by a detailed description of the core to determine the sedimentary sequence and quality of the productive intervals, and measurements from a Hollin sand outcrop located in the Andes Mountains to the northwest of the field.

Geostatistical methods were used for shale mapping. An objective geological model based on cores and outcrop was used to assign sand permeability, porosity and water saturation. Numerical simulation with this description and the steady state relative permeability data provided an oil rate forecast and the Plan of Development for the field.

Introduction

The Villano Field is located in Block 10 in the southwestern Oriente Basin, Ecuador. The block is on the western edge of the Amazon rain forest, approximately 33 km from the eastern foothills of the Andes Mountains and about 185 km by air, southeast of Quito. In the 1950's, the Villano 1 well was drilled near the crest of the structure. Drilling was stopped at 67 feet into the Main Hollin producing formation. Low oil gravity in the hydrocarbon shows apparently discouraged testing and further drilling at that time. ARCO, the current operator, acquired the block during a 1988 licensing round.

In 1992, Villano 2 was drilled down-dip of Villano 1 into the Main Hollin. Villano 2 produced 19° API oil at a commercially attractive rate from the Main Hollin. Coring was conducted with water-based

mud and Polycrystalline Diamond Compact (PDC), round profile core bits. Core recovery was only 47% because the core diameter was too small, apparently due to core bit and core barrel instability. The Villano 2 core did not provide valid connate water saturation. Produced brine samples from the aquifer contained 529 ppm total solids. Log-derived water saturation calculated using this brine and assumed Archie parameters gave average connate water saturation near 30%. This seemed high for clean, high-quality, sandstone with 200 feet of oil column with the water-oil density difference giving a gradient of 0.048 psi/foot. Mercury injection tests showed the average connate water saturation was indeed lower, about 17 %, with an expected transition zone of about 6 to 7 feet. The comparison between log and mercury injection estimates of connate water saturation can be seen in Figure 1.

The Villano crude oil is very undersaturated with a bubble point pressure of 190 psi with a gas oil ratio of 21 scf/bbl while bottom hole pressure is 4882 psig. The crude oil has 21° API stock tank gravity with a reservoir viscosity of 16.3 cp at 213° F bottom-hole temperature.

The Hollin sand is a crossbedded, quartzarenite sandstone (average 93.2% quartz) with porosity of 20% and permeability often greater than 1 Darcy. Pore space is primarily intergranular with a small percentage of secondary intragranular pores. The sandstones contain small amounts of authigenic kaolinite (average 2.7% total clay: 92% kaolinite, 7% illite, 1% chlorite) as localized clumps of book-like crystals, which appear to be formed by in-situ alteration of potassium feldspar. Quartz overgrowth cementation occurred early and prevented more severe compaction. Grain size ranges from fine-grained to very coarse-grained with only a trace of detrital clay. The rock can be heterogeneous with thinly bedded coarse or fine-grained sand laminae, which extend to the full diameter of the whole core. The Hollin sand has excellent quality.

The shale description was very important to depletion planning since it was expected that the reservoir would be produced by bottom-water drive. Coning of water into the producing wells can be significantly delayed by shale baffles. Unfortunately, incomplete recovery in the Villano 2 prevented reliable shale description from cores.

The need for reliable connate water saturation and shale description in the Hollin reservoir made it imperative to core a second well in the field to provide the data needed for depletion planning and calculation of hydrocarbon reserves. The low invasion coring method with water based coring mud would be used to provide water saturation data and the rock needed for lab tests to measure reservoir condition, water-oil relative permeability.[1,2,3] Oil-based mud, while still preferred for evaluating connate water saturation, was ruled out by the environmentally sensitive well location. This is one of ARCO's most complete examples of the value of low invasion coring using water-based mud for reservoir studies. It is also ARCO's first outside-the-USA application of low invasion coring. Protocols in the laboratory and at the well site have been improved since 1994. Several of these improvements will be described.

As a supplement to the core data, a study of a known Hollin outcrop was planned in the Andes to the northwest of the field to obtain a better idea of the shale types present, as well as their lateral extent and distribution. A shale map could then be provided by ARCO's stochastic shale generator after suitable conditioning with data from the outcrop, cores and well logs.

Operations at Villano #3

Coring Mud. Hole problems prevented the setting of the 9 5/8 inch diameter casing immediately above the coring depth. The casing shoe depth was 9183 feet, almost 2,600 feet above the coring depth. This left the Napo shales open to the well bore and required a high mud weight with chemical shale inhibition so that the well bore remained open for coring. Coring was being conducted in sidetrack #2. Drilling and well bore problems forced the abandonment of the earlier attempts. The original plan was to change the mud to a bland coring fluid at core point. This plan was abandoned when casing was set at a shallower depth than originally planned.

Coring Mud Formulation	
Water	0.85 bbl
Cationic PHPA	1.0 ppb
Cationic Low M.W. Copolymer	4.0 ppb
Biopolymer	0.75 ppb
Biocide	0.50 ppb
Starch, Modified	9.0 ppb
Cellulose fiber	12.0 ppb
KCl	35.0 ppb
Potassium bromide	0.30 ppb
Calcium carbonate	30.0 ppb
Barite	as needed
Fluid Properties	
Mud weight, lb/gal	10.8
pH	8.8
Solids Content, Vol. %	16
Plastic Viscosity, cp	34
Yield Point, lb/100ft^2	28
Gels(10 sec/10 min), lb/100ft^2	8/12
API fluid loss, cc	3.8
HTHP (200 F, 500 psi), cc	8.8
Potassium, ppm	30600
Chloride, ppm	43000

The 10.8 lb/gal mud weight would produce a hydrostatic pressure in the mud, which was 1800 psig greater than the formation. Fortunately, mud cake is compressible so the static fluid loss and spurt-loss were expected to be only about 25% greater than the values which would have been found at the lower hydrostatic pressure and mud weight with casing set just above core depth. While not ideal for obtaining a native-state core, experience suggested that low invasion coring could be used to minimize the problems caused by the non-ideal coring fluid.

When the coring depth was reached in the Upper Hollin, a mud centrifuge was used to decrease mud solids so that the sized calcium carbonate, 5 to 10 microns, cellulose fiber, and 2 lb/bbl additional starch could be added. Because of drill solids, barite and calcium carbonate, the total mud solids were 16% (vol.). This coring mud gave acceptable high-temperature, high-pressure, (HTHP) fluid-loss for low invasion. The potassium bromide tracer had been added earlier. Coring fluid samples were take at the beginning and end of each core from the suction pit. These were shipped with the core for tracer analysis.

Coring, Core Processing. Seven, 4-inch diameter cores were cut with low invasion core bits and 60-foot barrels with 100% core recovery. Coring rate ranged from 10 to 100 feet/hr with an average of 45 ft/hr. The lowest coring rate was at the start of each core. Total core length was 428 feet extending from the Upper Hollin through the water-oil contact in the Main Hollin. The aluminum inner barrels were cut into 3-foot lengths, sealed with rubber caps and steel hose clamps. The cores were then placed in wooden boxes and sent to the ARCO operations base about 30 minutes by helicopter from the drilling rig.

A commercial laboratory located in Bogota, Colombia imported the equipment and a cadre of 10 technicians to provide core sawing, plugging and preservation in a building constructed by ARCO for these operations. A geologist, reservoir engineer and lab technician from ARCO supervised this operation. Core plugs were cut from sawed lengths of whole core (3 inches for routine core analysis and 9 inches for special core analysis laboratory, SCAL, plugs) which were slabbed 1/4-3/4 to avoid moving filtrate by plugging fluid invasion from the more invaded outer radii. Each plug was cut into the center of the slab face. Invaded outer radii were removed from the plug by trimming. Routine horizontal core plugs 1-inch diameter by 2 inches long were cut every foot using refined oil as plugging fluid. Vertical routine core plugs the same size were cut every 10 feet with refined oil. Special core analysis laboratory (SCAL) plugs 1.5 inches diameter by 2 inches long were cut using 1000 ppm KCl brine as the plugging fluid. These plugs were cut 3 to 4 plugs side-by-side, from selected intervals containing the most uniform rock. The plugs were

preserved by placing them in glass bottles immersed in the plugging fluid. The plug containers were purged with nitrogen gas to remove as much oxygen as possible. The bottles were sealed and weighed to detect leakage while shipping. The whole core was preserved in Saran wrap, aluminum foil and CoreSeal. Packaging for shipping has been described in the literature and will not be repeated here[4]. Not a single core plug was lost due to bottle breakage in shipping. Core processing times were 4 to 6 hours for 60 feet.

The storage of the SCAL plugs under brine was the most acceptable solution available in this remote location. Anaerobic crude and humidified nitrogen gas are alternate fluids frequently used for SCAL plugging operations. These plugging fluids have the advantage that plug water saturation does not increase and no extraneous fluid is added to the core, which could cause a change in wettability. The Villano crude had too high viscosity at room temperature for use in cutting plugs and nitrogen was not considered for this operation. Humidified nitrogen gas is now the plugging fluid used for cutting both routine and SCAL plugs, but requires the use of a vacuum exhaust system to control the dust generated in this operation. The plugs are preserved in Saran wrap, aluminum foil, meltable plastic and Barax-aluminum foil heat-sealed laminate when nitrogen gas is used as the plugging fluid.

A commercial laboratory conducted routine analysis in the USA beginning about 10 days after coring was complete. Water saturation was determined by the Dean Stark method. After extraction with chloroform and drying in a vacuum oven to constant weight, the plug pore volume and permeability were measured in an automated device using gas expansion and pressure transients, respectively, at 800 psi net confining pressure. Every tenth plug was also measured at the estimated reservoir net confining pressure, 4500psi. The routine horizontal plugs were then crushed and extracted. The chloride and bromide in the core extract and in the mud filtrate was measured by ion chromatography.

Core Data for Villano 3

Mud Filtrate Invasion. The core and mud filtrate bromide data were used to calculate filtrate concentration in the Dean Stark water.[2] Bromide background in the formation brine varied from near 80 in the upper Hollin to about 3 ppm at water-oil contact. These are the minimum values observed and are similar to those which would be estimated if the ratio of bromide to chloride were similar to seawater. Bromide concentration in the mud decreased during coring from 1000 ppm to 700 ppm as the mud was diluted to control viscosity. The background bromide in the connate water had no significant effect on the calculated filtrate. Figure 2 gives the calculated filtrate saturation. The average value for filtrate saturation in the horizontal core plugs above the oil-water contact was 5.2% pv for those plugs with permeability exceeding 10 md. If the background bromide is taken as zero then this value becomes 5.7% pv. Permeability to air and coring rate are also shown in Figure 2.

Connate water saturation is calculated by subtracting the filtrate saturation from the water saturation measured by the Dean Stark method. The chloride concentration is calculated from equation (1):

$$C_{cw}^{Cl} = \frac{C_{ds}^{Cl} - FC_{mf}^{Cl}}{1-F} \qquad (1)$$

C_{cw}^{Cl} -Concentration of chloride in connate water, ppm

C_{ds}^{Cl} -Concentration of chloride in Dean Stark water, ppm

C_{mf}^{Cl} -Concentration of chloride in Mud Filtrate, ppm

F -Fraction of filtrate in Dean Stark water

These calculated values of connate water saturation and chloride concentration in the formation brine are given in Figure 3. The chloride concentration at the water-oil contact is 2600 ppm and at the top of the upper Hollin, 36,000 ppm. Apparently there is aquifer recharge from the Andes, where the Hollin outcrops. It appears the low salinity in the aquifer may be due to meteoric water from this recharge.

There is a trend in the chloride concentration with the amount of contamination by the mud filtrate. This is shown in Figure 4. The trend becomes more accentuated the lower the formation brine chloride. Both the bromide and chloride analyses were checked for analytical error by ARCO as possible causes of this variation. The values measured by the commercial laboratory were verified. The extrapolated values

have been used to generate Figure 5, which shows the variation in the chloride concentration with depth. Also included in that figure are measured chloride values for samples which had no evidence of filtrate contamination, i.e., zero bromide. They give similar values to those from extrapolation. An error function curve fits the data. Assuming the formation was filled with brine having 36,000 ppm chloride initially, the time to generate the chloride concentration gradient observed is about 200,000 years for a diffusion coefficient of 8×10^{-7} cm^2/sec. This indicates the low salinity in the aquifer could be relatively recent, but diffusion coefficients for the native state rock have not been measured so there is great uncertainty in this estimate.

When filtrate invasion is high, usually greater than 10% pv, it is found that connate water values begin to decline. This is caused in part by expulsion of the mixture of connate water and filtrate by the solution-gas-drive mechanism as the core is lifted to the surface and gas comes out of solution in the oil. Miscible displacement of the connate water may also occur as the mud filtrate invades to high values of filtrate saturation. The loss of connate water can be seen in Figure 6. When the fraction of filtrate in the Dean Stark water exceeds 0.5, or about 11.8% pv, the connate water saturation becomes lowered. For this reason, when calibrating logs or calculating J-function relationships the connate water saturation is only calculated for plugs for which filtrate in the Dean Stark water is less than half. The usual cut-off is about 10 % pv filtrate saturation, however, this will not hold for all rock and all values of connate water since it depends on relative permeability and displaceable saturation of hydrocarbons. A plot such as that shown in Figure 6 usually determines the cut-off.

The J-function in Figure 7 was generated with about 80% of the data above the water-oil contact. These are the samples that have low invasion with filtrate saturation less than 10%. A comparison is made between the connate water saturation from the low invasion core and that which would be estimated from the mercury injection data. There is reasonable agreement between the two sets of data. Low invasion core connate water saturation for the best rock, higher on structure is near 5% pv.

Special Core Analysis

Relative Permeability. The SCAL plugs for relative permeability tests were cut and stored under anaerobic brine in Ecuador. Screening permeability was then measured with anaerobic Villano crude (STO) at reservoir temperature, 215°F, and 500 psig, the normal procedure for low invasion core. These plugs were also screened by CT scanning.

Two composites were formed from two sets of 5 plugs each. The data on the composites are given in Table 1, below. Composite 1 consisted of coarse-grained, high permeability sandstone plugs from Core 3 (11,935.60 – 11,936.80'). Composite 2 consisted of medium-grained, intermediate permeability plugs from Core 4 (11,972.45 – 11,985.95'). Four additional plugs were used to measure water-oil imbibition capillary pressure. These plugs encompassed the entire permeability to oil at initial water saturation, $k_o(S_{wi})$, range (400 to 1500 md) observed in the screening. In order to expedite the capillary pressure measurement, the spontaneous brine imbibition step was skipped. A fifth plug was placed in an Amott cell at 155°F. After one year, there was no discernible imbibition of brine. Imbibition of STO was also near zero. Apparently the rock is very weakly wet.

A synthetic brine was formulated based on an average invasion-corrected chloride concentration of 11,650 ppm in the formation water for Cores 3 and 4. Calcium and potassium molar concentrations were assumed to be 10% of that of sodium. The compatibility of this brine with the rock was tested by unsteady-state waterflood on one of the remaining plugs at 215°F and 500 psig. The pressure drop across this plug was constant for 150 pv after oil production effectively ceased, indicating no rock-brine interactions.

Stock tank fluids were used for relative permeability testing because the oil in the reservoir is essentially dead. The filtered, dewatered, anaerobic crude was used in the waterfloods at 215°F. Due to the thermal limits of the centrifuge coreholder receivers, centrifuge displacements were conducted at 155°F. A portion of the filtered, dewatered anaerobic crude was stabilized at 165°F for the centrifuge tests. The centrifuge measurements indicate that water-oil capillary pressure is minimal over a wide saturation range. Forced oil imbibition on the centrifuge at the highest speed used in the capillary pressure measurement (3200 rpm) resulted in water saturations between 0.06 and 0.10. These values are comparable to the connate water saturations in the Core 3 rock. In the Core 4 rock, connate water saturation, S_{wc}, was 0.22.

The composite core tests were conducted at 215°F and 500 psig. Prior to injection of water, a crude oil tracer test was performed to independently measure oil-filled pore volume. At the end of the imbibition cycle, a brine tracer test was conducted to independently measure water-filled pore volume. If no further tests were required, the composite was then extracted and its routine properties were measured.

An unsteady-state (USS) waterflood was conducted in Composite 1 at an injection rate of 60 cc/hr. After 28.8 PV of injection, the rate was bumped first to 180 cc/hr, then to 540 cc/hr. The rate was then decreased in stages back to 60 cc/hr. Oil production continued during all but the last step, despite the injection of an additional 335 PV of brine. Water injection rate was increase to 9 times the original rate and then decreased back to the original rate. The relative permeability to brine increased from 0.2 to 0.7 in this process. The saturations from the unsteady state waterflood are given in the table below. The resulting relative permeability curves, which are rather unfavorable, are shown in Figure 8. The displacement was dominated by viscous instabilities induced by the large oil to water viscosity ratio of 40. The weak capillary pressure forces ensured that relaxation of radial saturation gradients did not occur during the waterflood. These curves are of little value since the displacement violated the stability criteria that must be met to calculate relative permeability from the production data. These results are a compelling reason for preferring the steady-state method for acquiring valid oil-water relative permeability (k_{row}-k_{rw}) curves for this reservoir.

An immobile initial water saturation was reestablished in Composite 1 by recirculating anaerobic STO at 215°F and 450 psig through the composite until P was constant and water production ceased in preparation for a steady-state (SS) test. A tracer test in crude oil was used to measure oil-filled pore volume. After equilibrium was achieved on the final step (water fractional flow, f_w, = 1), a tracer test was conducted again for measurement of water-filled pore volume. The relative permeability curves are given in Figure 8. The steady-state measurement yielded lower water and higher oil relative permeability than did the unsteady-state displacement. It should be noted that substantial volumes of brine were recirculated through the composite at each fractional flow setting, with 600 PV displaced just in the final step (f_w = 1). These large throughputs were necessary to establish saturation equilibrium at each water-oil ratio.

Table 1: Composite Test Results

Comp.	Perms. (md)	Test	PV cc	L cm	S_{wi}	S_{or}	Inj. (pv)	S_{or}(bump)	Inj.(bump) (pv)
1	1108-1282	USS	55.3	24.3	0.083	0.556	28.8	0.435	335
1	1108-1282	SS			0.108	0.415			
2	493-615	SS	56.1	25.0	0.162	0.361		0.359	

Precision of the saturation measurement by material balance is ±0.035 or better. Steady-state testing was also conducted on Composite 2. After equilibrium at f_w = 1, a rate bump (60 to 120 cc/hr) was performed which resulted in a very small reduction in oil saturation, in marked contrast to the bump after the unsteady-state displacement. The relative permeability to water was not significantly affected by this procedure. This change demonstrates that capillary pressure equilibrium had been established at the end of the f_w = 1 step. The relative permeability curves, also shown in Figure 8, are more favorable than those of Composite 1. Relative permeability to water, k_w, for Composite 2 is lower than that for Composite 1 at any given S_w. The explanation is that the rock in Composite 2 is more homogeneous than that in Composite 1.

That contrast was visually evident when the plugs were first mounted. Thin layers of very coarse-grained sand extend through the core plugs. Further confirmation of the heterogeneity is provided by a dispersion analysis of the tracer data. Much less dispersion occurred in both tracer tests performed on Composite 2 than on Composite 1. For the crude oil tracer test, the dispersion coefficients were 61 and 6 cm^2/hr for Composites 1 and 2, respectively. For the brine tracer tests, the corresponding values were 146 and 40 cm^2/hr. Despite the large throughput, the steady-state measurement did not reach low residual oil saturation or low oil relative permeability.

In order to extend the range of the relative permeability curves and measure the ultimate waterflood residual oil saturation, S_{orw}, centrifuge relative permeability to oil in a waterflood, k_{row}, measurements were made on four additional plugs picked from the original set of 30 screened plugs. This is appropriate since the oil production in the field will involve gravity drainage of oil upward as the water flows in from the aquifer below. These plugs had $k_o(S_{wi})$ values ranging from 520 to 2150 md. The average S_{orw} was 0.187 ±

0.035, which is substantially lower than that achieved with displacement. Once S_{orw} was attained, permeability to water at residual oil saturation, $k_w(S_{orw})$, was measured at 155°F and 500 psig. The resulting centrifuge k_{row} curves and $k_w(S_{orw})$ endpoints extend the displacement results in a consistent fashion, as demonstrated in Figure 8. The centrifuge and displacement data present an excellent example of how the steady-state displacement and centrifuge measurements complement each other.

Resistivity Measurements. Native-state resistivity core plugs (1.5 inches diameter by 2.0 inches long) were cut from the preserved whole core after the core arrived in the USA and about 2 months after coring. The plugging fluid was refined oil. The plugs were stored under plugging fluid until used for testing. The resistance was measured in a constant temperature bath at 140° F.

A native-state resistivity was measured on the plug with its as-received water saturation and formation water salinity. Water saturation was then measured using Dean Stark analysis, followed by cleaning with chloroform, extraction of salt with water, displacement with methanol, drying, pore volume measurement by gas expansion. The salinity of the formation brine was calculated from the Dean Stark water volume and by measuring the extracted salts. From this salt concentration, a value for brine resistivity was estimated. The plug was then resaturated with brine containing 178,000 ppm sodium chloride and 2700 ppm calcium chloride. Resistivity was measured after flow and equilibration with the brine at four different brine salinities which showed clay conductivity was negligible. The formation resistivity factor from these tests was used to calculate the resistivity of the plug when 100% saturated with the formation brine found in the plug. The value of the Archie cementation exponent, m, was 1.74 with the constant, a = 1.

Restored-state resistivity was measured on a separate group of core plugs, in order to extend the range of water saturations. These were first extracted with chloroform-methanol azeotrope, dried, pore volume was measured by gas expansion, and then the core plug was resaturated with the same initial brine as above. The procedure summarized above was used to evaluate Archie cementation exponent. The restored-state plugs were then flooded with refined oil and resistivity index was determined. A plot of the Archie saturation exponent, n, is given in Figure 9 for both the native-state and restored-state protocols. The observed variation of n with water saturation was built into the log interpretation model.[5] While the samples are not highly microporous, the microporosity that is present is highly correlated with the level of kaolinite clay minerals. On the average, the pore space less than 2 microns comprises about 10 % of the pore space but varies from as little as 2 % to as much as 20% of total, based on mercury injection experiments.

It must also be stated that an oil drive for establishing water saturation in resistivity index testing is no longer used because of saturation gradients remaining in the core plug. Porous plates with a nitrogen drive are now used to desaturate core plugs for resistivity index tests.

Mercury injection tests and x-ray diffraction data were measured after resistivity testing.

Comparison of Villano 3 Cores and Well Logs

The well log interpretation method described below was applied to the Villano 2 and Villano 3 wells. The borehole-corrected total gamma-ray log was used to calculate clay volume with a clay value of 200 API and a sand value of 45 API. Porosity was calculated from the borehole corrected bulk density log (matrix density = 2.66 g/cc and fluid density = 1.0 g/cc) with correction for clay effects using the gamma-ray clay volume and a clay porosity of 0.08. The laboratory measured value of m and n which were discussed above have been used in the Simandoux equation with the clay resistivity value, 3.0 ohm meters, obtained in the overlying Napo shales. The Villano 3 chloride concentration varied from 36,000 ppm at the top of the Hollin to 2600 ppm at the water-oil contact, according to the diffusion curve in Figure 5. Formation brine resistivity was then estimated from the equivalent sodium chloride concentration. The diffusion curve was truncated at the top when the pay zone was not as thick as that found in Villano 3, so that salinity at the top of the pay zone declined as the pay thinned at the edges of the field. The salinity at the water-oil contact was held constant. The variation of n with water saturation required an iterative solution. The starting value for n was taken as 2.0 and a value of water saturation was calculated. A new value of n was then estimated from Figure 9 data and this was repeated until the difference between consecutive calculations of water saturation was less then 0.0015.

The comparison of the Villano 3 well log derived water saturation and low invasion cores are given in Figure 10. The agreement is excellent. The contrast between the log-derived water saturation in the two Figures 1 and 10 should be noted. The water saturation varies from 5 to 6 % pv at 11834’ to about 20 % pv

just above the water-oil contact. The mean core water saturation is 9.96% pv and the mean log derived water saturation is 9.84% pv. It is estimated the standard deviation of water saturation from cores is about ±4 % pv and about ±10 % pv for the well logs. The standard error of the mean will be (standard deviation)/(number of feet) ^0.5. In the numerical model, capillary pressure curves giving the same water saturation as the Villano 3 cores and logs was used to initialize the model.

Stratigraphy and Depositional Environment

About 5 km of Mesozoic and Cenozoic sediments are preserved in the Villano Field. The lower most unit is the Lower Cretaceous Chapiza Formation, which consists of a thick series of continental redbeds and volcanic deposits. Figure 11 shows a stratigraphic section for the Villano Field. This is overlain by fluvial quartz arenite sandstone of the Main Hollin formation, which is overlain by the shallow marine transgressive clastics of the Upper Hollin. The Napo shale conformably overlies the Upper Hollin. The Villano 3 core was described in detail to provide an understanding of the depositional environment within the Main Hollin. The lower part of the Main Hollin was deposited in incised valleys cut into the Chapiza formation, and consists of a thick series of braided stream deposits with excellent reservoir quality. The bulk of this unit is water bearing in the Villano Field. The upper part of the formation, which contains the majority of the oil in the Main Hollin, is interpreted to have been deposited in a sandy meandering river system. The point bars of the meandering river deposits are excellent quality sandstones, while thicker beds of poorer quality are common in the upper part of the Main Hollin and are interpreted to be crevasse splay, levee and chute fill deposits.

Hollin Outcrop Study

A detailed study of three outcrop sections of the Hollin formation along the Loreto-Coca Road was undertaken to obtain additional geologic data to develop a reservoir description to be used in a reservoir simulator. The outcrop locations are about 50 kilometers northwest of the Villano Field in a paleodepostional basinward setting. Figure 12 is a montage showing sections at the measured locations and log response.

The three outcrop locations are aligned east to west, with a distance of 0.5 kilometers between locations 1 and 3, and 4 km between locations 1 and 2. At sections 1 and 3 the Main hollin formation overlies the Chapiza unconformity and the Upper Hollin is present above the Main Hollin, which allowed the placement of the various facies within the Main Hollin to be observed. At location 3 the contact with the Napo shales was also observed, but the Chapiza was not.

The outcrop sections at each location were photographed, described in detail and sampled. A gamma ray log was measured using a hand held scintillometer. Thin sections were cut from 75 samples to measure and understand mineralogy and log response for each facies. The outcrops were photographed and shale type, size and distribution were measured.

The depositional environments in the outcrops have similar sedimentary structures and individual unit thickness as those observed in cores from the Villano Field. The Main Hollin in the outcrops consists of braided stream, point bar and transitional marine sands as in the Villano Field, although the overall thickness of each unit is less in the outcrop. Four primary types of impermeable barriers or baffles occur in the outcrop and in the field; (1) bar tops or mud flats within the braided stream environment; (2) overbank, floodplain or levee silts and clays; (3) abandoned clay-filled channels within the point bar sands; and (4) clay drapes within the upper point bars. In the Villano Field, fine-grained restricted bay deposits are present in the Upper Hollin and chute filled deposits are present in the Main Hollin.

A stratigraphic model of the Main Hollin formations was developed using interpreted depositional environments from core and wireline log data in the Villano and Moretecocha (a Hollin discovery, about 11 miles south-southeast of Villano) Fields and from measured sections of the outcrop study. The objective was to derive a geologically sound model of the stratigraphic variation to be expected within the Main Hollin formation. Based on the preserved thickness of up to 50 feet in the individual point bar deposits in the field, the size of the meandering river system of the upper part of the Main Hollin formation is in the same order of magnitude as the present day Mississippi River system in the United States. An areal photograph of a representative portion of the Mississippi River system could then be used to estimate the relative frequency of occurrence of point bar deposits, overbank levee deposits, preserved floodplain

deposits, crevasse splays, chutes and abandoned channels or oxbow lake deposits. The less complex braided stream of the lower part of the Main Hollin was modeled using standard published facies models for such systems. The resulting cross section was representative of the stratigraphic variation likely to occur in any vertical slice though the field and was used as a basis for the reservoir simulator description.

Geostatistical Shale Mapping and Reservoir Simulator Description

Shales in the Villano reservoir represent barriers or baffles to vertical flow, which will significantly impact oil recovery under the expected bottom-water drive mechanism. A realistic description of the shales was necessary to predict oil rate and recovery in the reservoir simulator, and confirm the economic viability of the proposed development scenario.

The shale body sizes and distribution determined from Villano cores, the outcrop study and the stratigraphic model were incorporated into ARCO's Stochastic Shale Generator program, which generates multiple descriptions of the shales which honor the data.[6] The program inputs include probability distributions for the thickness, length, width and frequency of the various types of shales observed in the Hollin depositional environments. The output includes transmissibility modifiers for each grid-block that are directly read into the reservoir simulator.

Ten types of shales with widely varying dimensions were defined to describe the shales occurring in the three main depositional environments of the Hollin formation; (1) marine/transition, (2) meandering river, and (3) braided stream. The shale dimensions were defined using triangular probability distribution functions that account for the minimum, most likely, and maximum values of each dimension. Figure 13 shows a sample of a triangular distribution function for floodplain shales. A wide variation in shale types and sizes was necessary to develop a description consistent with the geological model.

In addition to the size, the frequency of occurrence of the shales was incorporated into the model, using volume fractions of each type of shale by model layer, which were determined by the depositional facies present in the layer. A volume fraction of zero for any shale indicated that shale was not present in that layer. For shales that were present, the volume fraction is defined as the volume of shale type in the layer divided by the total volume of reservoir in the layer. Only size and volume of shale was used in this stochastic model; no orientation was specified. The shale model was conditioned using the shales observed in the Villano 2 and Villano 3 cores.

The stochastic shale generator calculates the effective vertical transmissibility for each simulator gridblock, which allows the effect of the shales on vertical flow to be modeled. The permeability factors range from zero to one, so that when no shales are present in a gridblock, the permeability factor is one. A gridblock partially covered by shales will have a permeability factor between zero and one depending on the size of the shales and their position within the block, while a gridblock completely covered by a shale will have a permeability factor of zero. Since the stochastic shale generator provides multiple descriptions that honor the data, the most likely description was chosen as the one that most closely resembled the stratigraphic cross section developed by the geologists. The shale description as it appeared in the simulator is shown in Figure 14. This figure shows all the shales on the left side and only the larger shales on the right side.

Reservoir Simulation and Predicted Performance

The reservoir description and laboratory data were incorporated into ARCO's reservoir simulator to predict performance of the field under different development scenarios. The original oil in place was calculated using a structure map derived from seismic data, with rock properties and fluid saturations determined wireline logs tuned to the core data. The 3-D reservoir model was built using ARCO's reservoir simulator. The model contains 21,528 gridblocks, with 23 vertical layers, which are 10' thick in the oil column to model coning behavior. The areal grid is of varying size, with the minimum cell size of 600' x 300' over the expected producing area of the field. Porosity and permeability were obtained from core data. Water saturation was then calculated from the well logs calibrated with the core data. Fluid properties were available from PVT data measured on bottom-hole samples and relative permeability came from steady-state measurements on Villano 3 low invasion composite cores as described earlier.

There were two key inputs to the reservoir model that had a large impact on the predicted field performance, the shale description and the relative permeability data. Due to time constraints, the unsteady

state relative permeability data, which takes less time to measure, were tried in the simulator. These curves were highly unfavorable and inaccurate, due to viscous effects described earlier, and resulted in a reserve prediction for the field that was uneconomic. It was then decided to defer the study until the steady-state data were available. The first few data points from the first steady-state composite, supplemented by data at high water saturations from another ARCO field with similar fluid properties and wetting characteristics, provided sufficient data to develop a relative permeability curve for the simulation. This curve was later confirmed after the steady state measurements were completed. The data from composite 2 were incorporated into the model later, resulting in a higher final rate prediction on which the current development plan is based.

The reservoir simulator showed that depending on the nature and placement of the shales, the model predicted that the wells could produce under either bottom water or edge water drive, or both, depending on the well's proximity to one of the larger shales. Because of the uncertainty in the actual shale description, either mechanism is possible at any point in the reservoir. Early production of water in the up-dip wells is as likely as it is for the down-dip wells. Therefore, it was recognized that the well plan needed to be flexible in order to adapt to the water influx pattern, indicating that high angle wells with the capability to produce from multiple zones would be needed.

Current Status of Field Development

The Villano Field is currently under development and is expected to start up in mid-1999. The well plan calls for recompleting wells Villano 2 and 3, and drilling five high angle wells to produce a plateau rate of 40,000 STBD. Produced water will be disposed of in a well completed in the aquifer. The field will be developed without the use of roads, with all equipment to be brought in by helicoptor. The high angle wells will be drilled from a single well pad to minimize the amount of space required in this sensitive rain forest environment.

The integrated study using the Villano 3 core data and the description efforts, including the outcrop study were key to the development plan for this field. The discovery of the water salinity gradient and the variable saturation exponent provided a basis for determining water saturation from wireline logs. The relative permeability data and shale description had a large impact on the predicted oil and water production. The potential edge water drive mechanism indicated the need to be able to complete the wells within multiple intervals to produce oil located between large shale bodies, resulting in the decision to drill high angle rather than strictly horizontal wells. Although there is still uncertainty in the water production predictions, the results from this study provided a sound basis for facility design and confirmed the economic viability of the field**.**

Conclusions

1. Salinity varied from the top to the bottom of the reservoir. Coring is the only method to obtain such information.
2. Water-based mud low invasion coring yields reliable connate water saturation and improved agreement between core data, logs and mercury injection data.
3. Unsteady state waterflood gave a poor estimate of water-oil relative permeability due to viscous fingering and core plug scale heterogeneity.
4. The steady state method of relative permeability measurement leads to prediction of higher oil recovery in high mobility ratio waterflood
5. Centrifuge and steady state measurement methods give similar curves for relative permeability.
6. Outcrop studies were essential to prediction of edge-water and bottom-water drive performance.
7. The engineering study and plan of development for the Villano Field could not have been reliably completed without the carefully designed and executed coring and data acquisition plan.

Acknowledgments

The authors thank ARCO Oriente, Inc., AGIP Petroleum (Ecuador) and Petroecuador for permission to publish these results. The contents and conclusions in this paper are those of the authoring company and may not be shared by the other working interest owners. We acknowledge the contributions of Hughes-Christensen for the coring bits, Baker Hughes INTEQ for field operational support, Core Lab, Bogota and

Dallas for the core handling, preservation and analysis and the ARCO drilling staff. We thank the numerous people in ARCO Oriente, Inc., ARCO Exploration and Production Technology and ARCO International Oil and Gas Company who made significant contributions to the success of this project.

References

1. Rathmell, J. J., Tibbitts, G. A., Gremley, R. B., Warner, H. R. Jr., and White, E. K., "Development of a Method for Partially Uninvaded Coring in High Permeability Sandstones," SPE 20413 presented at the SPE Annual Technical Conference and Exhibition in New Orleans, La., 23-26 September, 1990, SPE Formation Evaluation, June 1995, 65-71.
2. Rathmell, J. J., Gremley, R. B. and Tibbitts, G. A., "Field Applications of Low Invasion Coring," SPE 27045, Presented at LACPEC III, Buenos Aires, Argentina, 27-29 April, 1994.
3. Rathmell, J. J., Gale, B. A., Tibbitts, G. A., Bobrosky, D. J., Wilton, B. S. and Bell, D. A., "Development and Application of PDC Core Bits for Down-hole Motor Low Invasion Coring in the Arab Carbonates", SPE 36263 presented at the 7th ADIPEC held in Abu Dhabi, 13-16 October, 1996, SPEDC, March 1998.
4. Rathmell, J. J., Bloys, J. B., Bulling, T.P., Parr, J. J., Pasternack, E. S., Jerauld, G. R., and Sakurai, S., "Low Invasion, Synthetic Oil-Base Mud Coring in the Yacheng 13-1 Gas Reservoir for Gas-in-Place Calculation" SPE 29985 Presented at the 1995 International Meeting on Petroleum Engineering held in Beijing, China, 14-17 November, 1995.
5. Worthington, P. F. and Pallatt, N., "Effect of Variable Saturation Exponent upon the Evaluation of Hydrocarbon Saturation", SPE 20538, Presented at the SPE Annual Technical Conference in New Orleans, La., 23-26, September, 1990.
6. Perez, G., Chopra, A. K. and Severson, C. D. "Integrated Geostatistics for Modeling Fluid Contacts and Shales in Prudhoe Bay," paper SPE 26475, presented at the Society of Petroleum Engineers Annual Technical Conference and Exhibition, Houston, Texas, 3-6 October, 1993.

Figure 1: Villano 2 logs give high Sw compared to mercury injection.

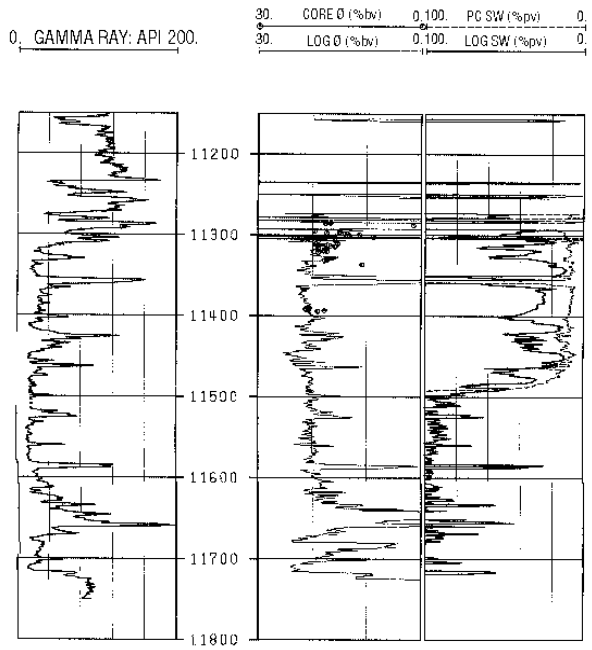

Figure 3: Connate water saturation and formation brine chloride after adjustment for invasion by mud filtrate.

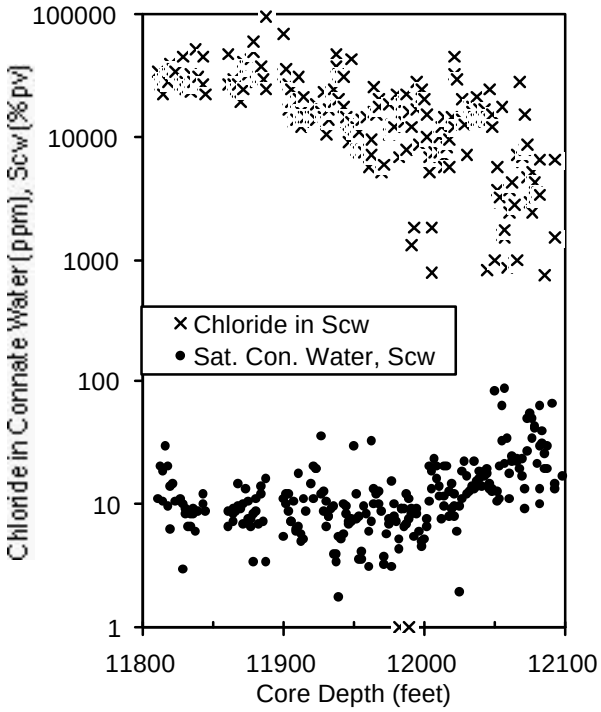

Figure 2: Villano 3 core properties, coring rate and invasion

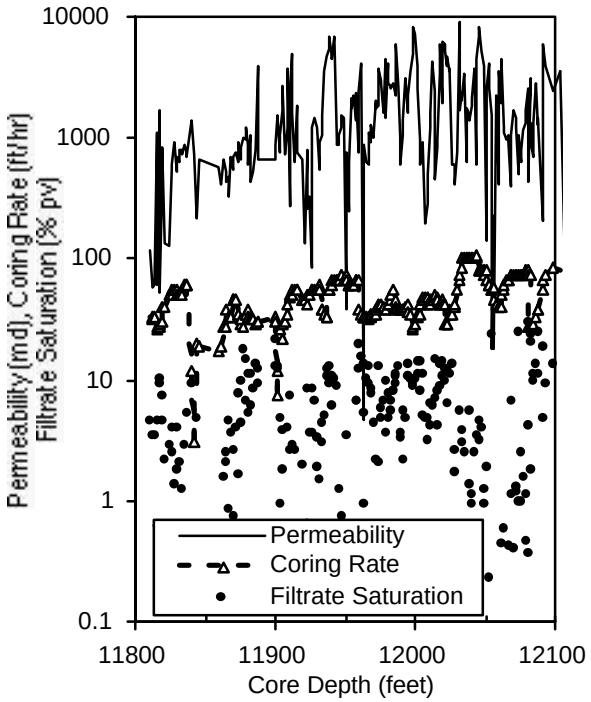

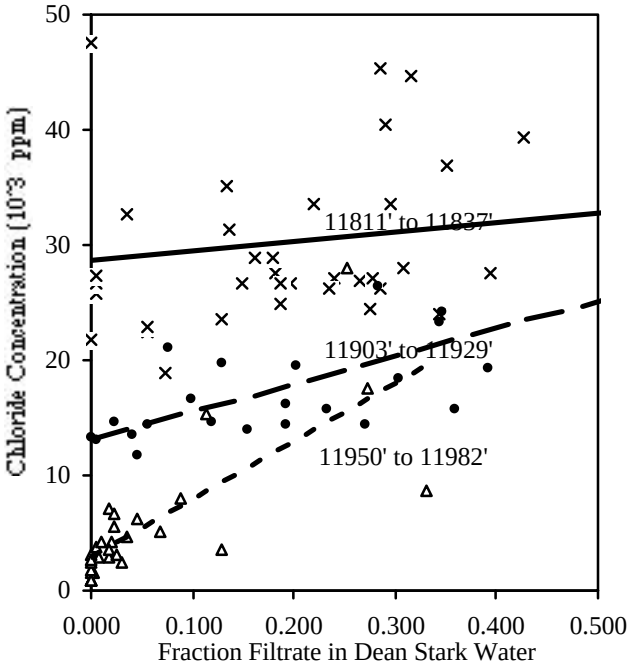

Figure 4: Variation in filtrate adjusted formation brine chloride with level of mud filtrate invasion.

Figure 5: Variation in formation brine chloride with depth

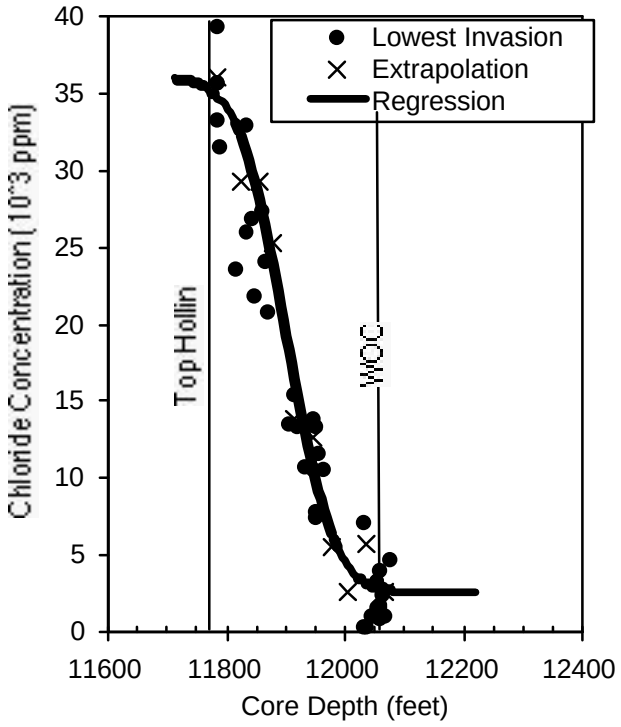

Figure 6: Loss of connate water by solution-gas-drive during lifting.

Figure 8: Reservoir condition water-oil relative permeability from the Villano 3 composites.

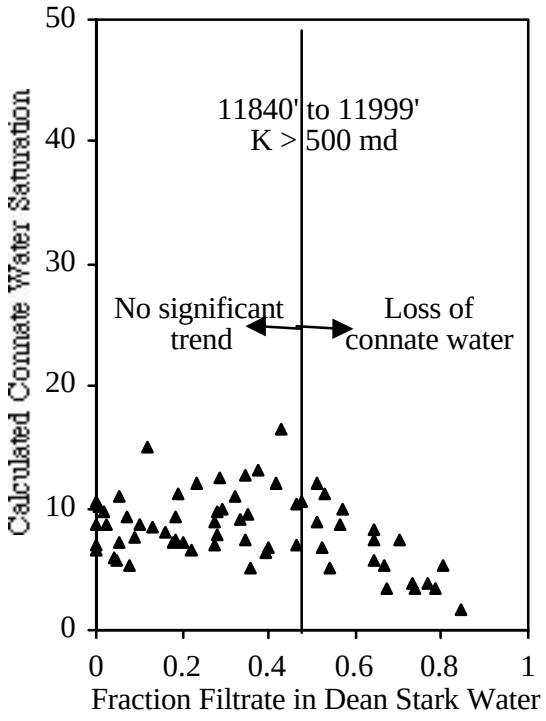

Figure 7: J-Function from the Villano 3 low invasion core connate water saturation compared tomercury injection.

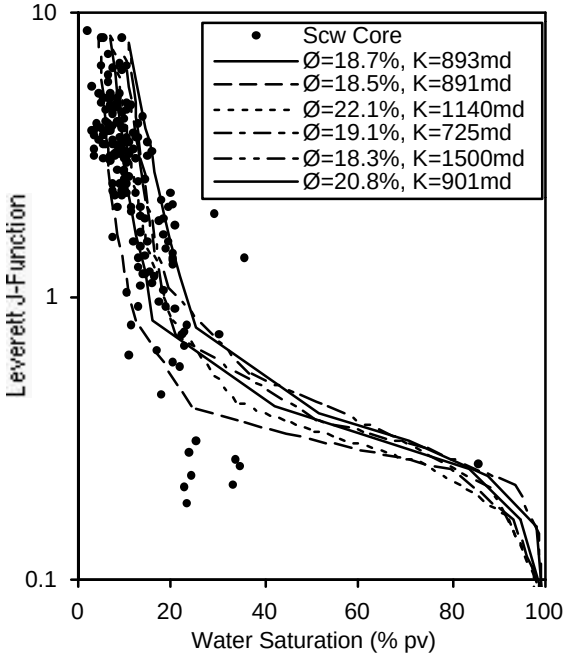

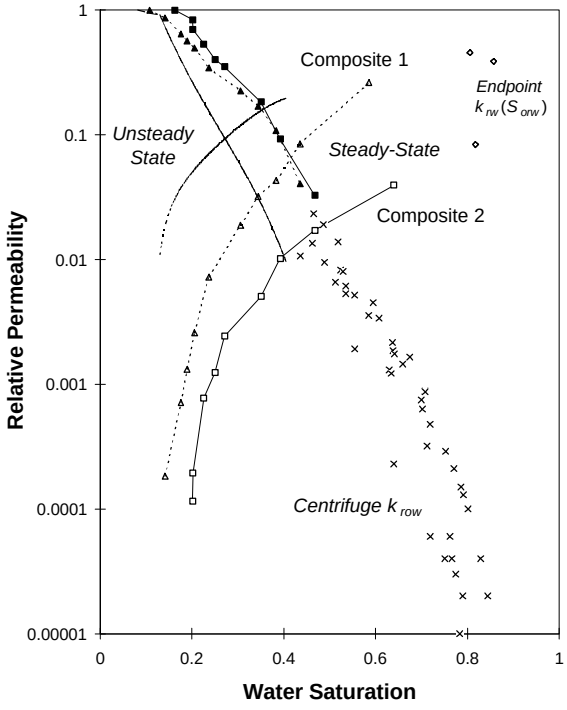

Figure 9: Archie saturation exponent measured by native-state and restored-state methods on the Villano 3 core plugs.

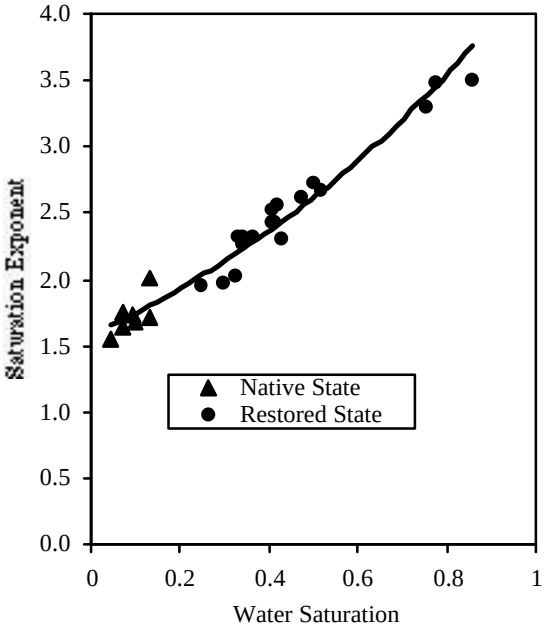

Figure 10: Water saturation from Villano 3 well logs and cores

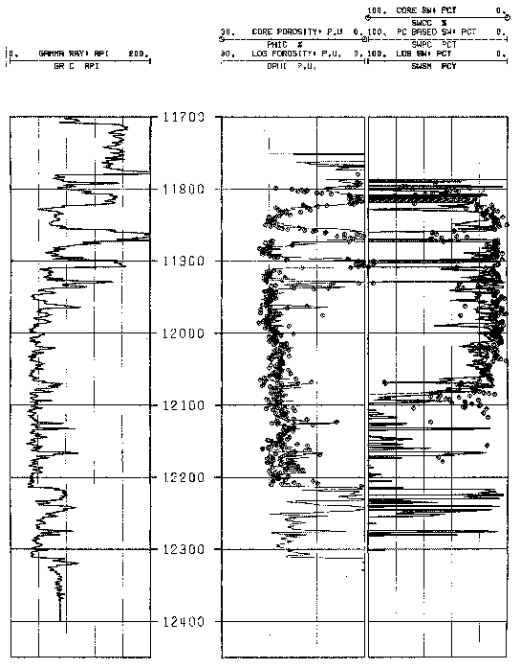

Figure 11: Stratigraphic Section of the Villano Field

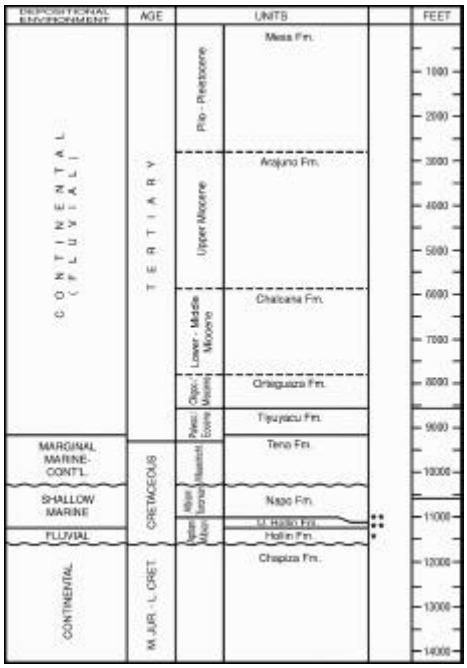

Figure 12: Cross section of Hollin outcrop showing shale type and distribution with gamma ray log response

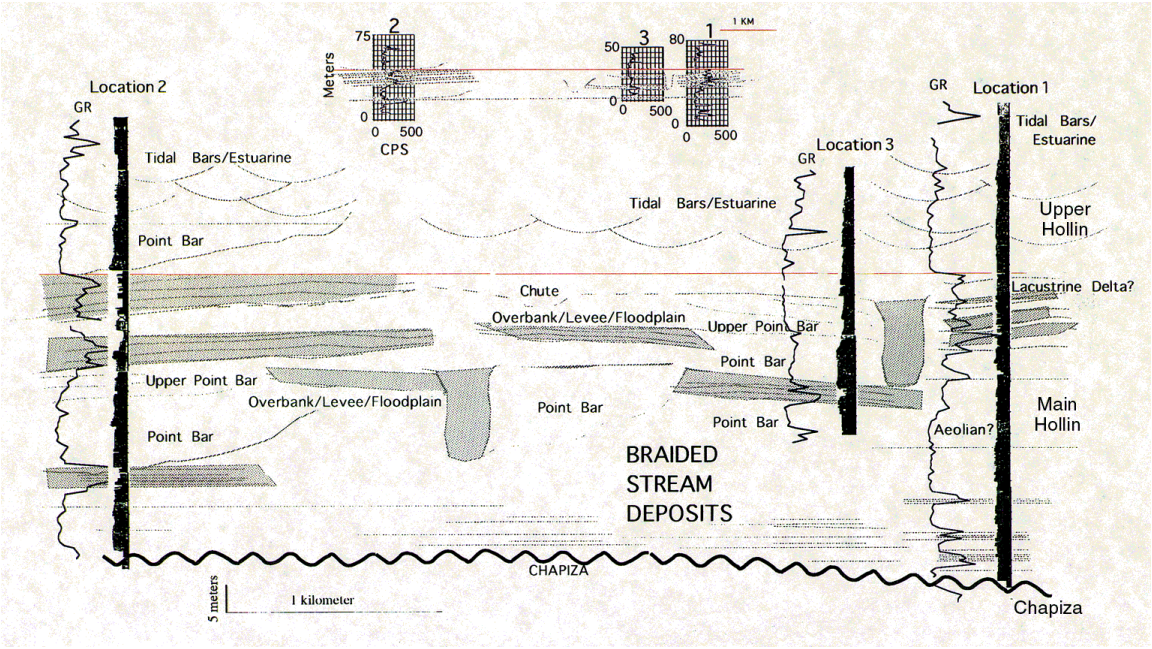

Figure 13: Distribution functions for floodplain shale dimensions in geostatistical shale generator

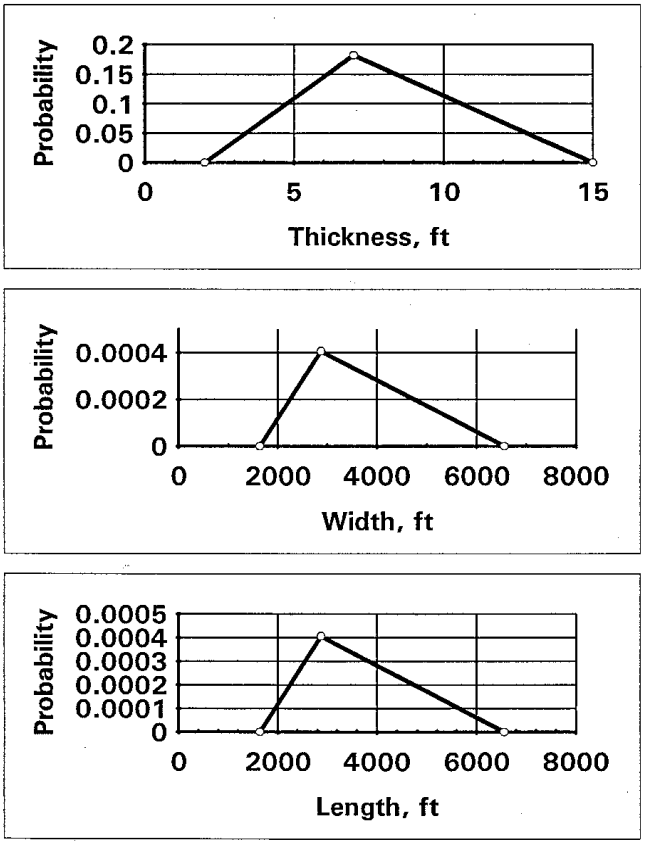

Figure 14: Shales at they appeared in the model, left side, composite of all shale types, right side, largest shale types